

# Impurity effects on BCS-BEC crossover in ultracold atomic Fermi gases

Yanming Che and Qijin Chen\*

*Zhejiang Institute of Modern Physics and Department of Physics,  
Zhejiang University, Hangzhou, Zhejiang 310027, China and*

*Synergetic Innovation Center of Quantum Information and Quantum Physics, Hefei, Anhui 230026, China  
(Dated: October 1, 2018)*

We present a systematic investigation of the effects of “nonmagnetic” impurities on the  $s$ -wave BCS-BEC crossover in atomic Fermi gases within a pairing fluctuation theory. Both pairing and impurity scattering  $T$ -matrices are treated self-consistently at the same time. While the system is less sensitive to impurity scattering in the Born limit, for strong impurity scatterers, both the frequency and the gap function are highly renormalized, leading to significant suppression of the superfluid  $T_c$ , the order parameter and the superfluid density. We also find the formation of impurity bands and smearing of coherence peak in the fermion density of states, leading to a spectrum weight transfer and finite lifetime of Bogoliubov quasiparticles. In the BCS regime, the superfluidity may be readily destroyed by the impurity of high density. In comparison, the superfluidity in unitary and BEC regimes is relatively more robust.

PACS numbers: 03.75.Ss, 03.75.Nt, 74.20.-z, 74.25.Dw

## I. INTRODUCTION

Ultracold atomic Fermi gases have been a rapidly growing field over the past decade, and have attracted enormous attentions from various disciplines including condensed matter, atomic and molecular physics, nuclear matter and astrophysics. Owing to the high tunability of multiple parameters, atomic Fermi gases have become a prototype for quantum simulations of a vast range of existing quantum systems in, e.g., condensed matter and for engineering highly exotic quantum states [1]. One such system is superconductors with a tunable interaction strength. Despite that atomic Fermi gases can be prepared as a clean system without an impurity, impurities are hard to avoid in a typical condensed matter system, including the most important and widely studied high  $T_c$  cuprate and Fe-based superconductors. Therefore, study of the impurity effects on the superfluidity and pairing phenomena using an atomic Fermi gas is very important.

Associated naturally with a two-component Fermi gas is the physics of superfluidity and pairing, whose counterpart condensed matter system is superconductivity. The related impurity effects in superconductors have also been an important subject, including superconducting alloys[2], disordered high  $T_c$  superconductors[3, 4], disordered superconducting thin films and the disorder induced superconductor-insulator transition [5–8], etc. While the impurity effects in conventional phonon-mediated  $s$ -wave superconductors have been understood fairly well, the pseudogap phenomena in ( $d$ -wave) cuprate superconductors have introduced further complexity [9]. Unlike a typical superconductor, the pairing interaction strength in atomic Fermi gases can be tuned via a Feshbach resonance from weak to strong, effecting a crossover from BCS superfluidity to Bose-Einstein condensation (BEC).

Pseudogap phenomena have been widely recognized as the pairing strength become strong. It is thus interesting to go beyond weak coupling BCS theory and study the impurity effects in the presence of strong pairing. Indeed, experimentally, impurities can be introduced via doping atoms of foreign elements [10] or using a random optical potential [11].

In a conventional  $s$ -wave BCS superconductor, weak impurities renormalize the frequency  $\omega$  and gap  $\Delta$  in the exact same fashion [12], such that their effects are canceled out in the gap equation, leading to the Anderson’s theorem [13], with an unchanged superconducting transition temperature  $T_c$ . For a  $d$ -wave superconductor, it has been known that impurities often lead to a quadratic temperature dependence for the low temperature London penetration depth or superfluid density. Chen and Schrieffer [4] have studied the effects of nonmagnetic impurities for a  $d$ -wave superconductor on a quasi-two-dimensional lattice from the Born to unitary limits of the impurity scattering strength, and for both weak and strong pairing strengths. On the other hand, since no strong pairing  $s$ -wave superconductors have been found thus far, there has been very few studies of the impurity effects in strong pairing  $s$ -wave superconductivity. Orso studied BCS-BEC crossover in a random external potential [14], based on the Nozieres and Schmitt-Rink (NSR) theory [15], which has been known to suffer from inconsistencies between its  $T_c$  equation and fermion number equation in terms of the self-energy contributions of pairing fluctuations. Han and Sa de Melo [10] studied the BCS-BEC crossover in the presence of disorder, using functional integrals and a local density approximation, which requires the interaction range of the disorder be much larger than the pair size. Recently, Strinati and coworkers [16] studied the impurity effects in the context of BCS-BEC crossover, but at the lowest order, using a diagrammatic approach, which does not have a pseudogap in the  $T_c$  equation even in the strong pairing regime, where the presence of a pseudogap has been established experimentally. At the same time, higher order contributions from impurity scat-

---

\*Corresponding author: qchen@zju.edu.cn

tering in the strong scattering regime are missing in their treatment, and the impurity and pairing  $T$ -matrices are not treated in a self-consistent fashion, either.

In this paper, we will present a systematic treatment of the impurity effects on a two-component ultracold atomic Fermi gas as a function of the impurity strength, impurity concentration, and pairing interaction strength, in the case of  $s$ -wave pairing throughout the BCS-BEC crossover. We will use the formalism developed in Ref. [4], where the pairing fluctuations and nonmagnetic impurity  $T$ -matrix are treated self-consistently. While the original formalism was applied to  $d$ -wave pairing on a quasi-two-dimensional lattice, relevant to cuprate superconductors, here we apply it to  $s$ -wave pairing throughout the entire BCS-BEC crossover in a three dimensional (3D) atomic Fermi gas. Unlike the nodal  $p$ -wave [17] and  $d$ -wave cases [4], where the gap renormalization vanishes, for the  $s$ -wave pairing, both of the frequency and gap renormalization induced by impurities are present. Only for weak impurity scattering (i.e., the Born limit), where the impurity potential may be treated at the Abrikosov-Gor'kov (AG) level, the frequency and gap renormalization factors are exactly the same so that the Anderson's theorem is valid [12, 18].

Our main results are as follows: (a) In the presence of strong impurity scattering, the frequency and the gap function are highly renormalized, leading to significant suppression of the superfluid  $T_c$ . (b) In the BCS regime, impurities induce impurity bands, subgap states and strong smearing of the coherent peak (CP), thus the superfluidity may be readily destroyed by the impurity. Besides, we find an effective power law dependence of  $T_c$  as a function of pairing strength [19]. (c) Superfluidity in the unitary and BEC regimes is relatively more robust than in the BCS regime. (d)  $S$ -wave pairing is less sensitive to impurity than its  $d$ -wave counterpart [4]. (e) Strong impurity scatterers are much more effective than weak scatterers in the Born limit, in suppressing  $T_c$ , order parameter, and the superfluid density.

It should be noticed that there are also other theoretical approaches toward the interplay of BCS-BEC crossover and impurity, mainly using functional integral formalism and the replica trick [10, 14].

The rest of this paper is arranged as follows. In Section II we briefly recapitulate the theoretical formalism developed in Ref. [4], with a focus on the main results and the differences between the  $s$ -wave atomic Fermi gases and the  $d$ -wave cuprate superconductors. In Section III we numerically solve the set of equations to get various impurity renormalization effects on density of states (DOS),  $T_c$ , gaps, and superfluid density, etc, throughout the BCS-BEC crossover. Finally we discuss the results and experiment related issues.

## II. THEORETICAL FORMALISM

### A. Frequency and gap renormalizations

The formalism for BCS-BEC crossover at finite temperature in a clean system can be found in Section II(A) of Ref. [4]. Here for atomic Fermi gases of  $^6\text{Li}$  or  $^{40}\text{K}$ , we

take the free fermion dispersion  $\epsilon_{\mathbf{k}}^0 = \mathbf{k}^2/(2m)$ , and a contact potential for the  $s$ -wave pairing interaction  $V_{\mathbf{k},\mathbf{k}'} = g\varphi_{\mathbf{k}}\varphi_{\mathbf{k}'}$ , with  $\varphi_{\mathbf{k}} = 1$ , where  $m$  is the atomic mass and we take  $\hbar = k_B = 1$  as usual. The ultraviolet divergence in the gap equation, caused by the unphysical contact potential, can be regularized in a standard way so as to replace  $g$  with  $1/k_F a$  using the Lippmann-Schwinger equation [1]

$$\frac{m}{4\pi a} = \frac{1}{g} + \sum_{\mathbf{k}} \frac{1}{2\epsilon_{\mathbf{k}}^0}, \quad (1)$$

where  $k_F$  is the Fermi wave vector and  $a$  is the two-body  $s$ -wave scattering length. Now by solving self-consistently the gap equation, atomic number equation and pseudogap equation, one can study BCS-BEC crossover at finite temperature in atomic Fermi gases as a function of  $1/k_F a$ .

The impurity Hamiltonian is given by

$$H_I = \sum_i \int d\mathbf{x} \psi^\dagger(\mathbf{x}) u(\mathbf{x} - \mathbf{x}_i) \psi(\mathbf{x}), \quad (2)$$

with  $u(\mathbf{x} - \mathbf{x}_i) = u\delta(\mathbf{x} - \mathbf{x}_i)$ , where  $\mathbf{x}_i$  denotes independent, randomly distributed impurity sites. We refer to these impurities as “nonmagnetic” in the sense they cannot convert one species of atoms into the other, similar to a superconductor where a nonmagnetic impurity does not cause spin flips.

At the AG level [2, 12], impurities in a  $s$ -wave BCS superconductor only induce frequency and gap function renormalization, leading to the Anderson's theorem for weak impurities. In Ref. [4], Chen and Schrieffer went beyond the AG level, and considered impurities of arbitrary strength and variable pairing interactions by treating the impurity  $T$ -matrix and pairing fluctuations self-consistently at the same time. Now we shall present the main results of the formalism, while detailed derivations can be found in Ref. [4].

The frequency and gap renormalizations now are given in terms of the impurity  $T$ -matrices,  $T_\omega$  and  $T_\Delta$  (and its complex conjugate), by

$$i\tilde{\omega} = i\omega - \Sigma_\omega, \quad i\tilde{\omega} = -i\omega - \Sigma_{-\omega}, \quad (3a)$$

$$\tilde{\Delta}_{\mathbf{k}} = \Delta_{\mathbf{k}} + \Sigma_\Delta, \quad \tilde{\Delta}_{\mathbf{k}}^* = \Delta_{\mathbf{k}}^* + \Sigma_{\Delta^\dagger} \quad (3b)$$

where  $\Delta_{\mathbf{k}} = \Delta\varphi_{\mathbf{k}}$ ,  $\Sigma_\omega = n_i T_\omega$  and  $\Sigma_\Delta = n_i \Delta T_\Delta$ , with  $n_i$  being impurity density. Here  $\tilde{\omega} = (-\omega)$ . Now except that  $i\tilde{\omega}$  and  $\tilde{\Delta}_{\mathbf{k}}$  acquire new expressions, the Green's function  $G$ , Gor'kov function  $F$ , and the pair susceptibility  $\chi(Q)$  remain formally the same in terms of  $i\tilde{\omega}$  and  $\tilde{\Delta}_{\mathbf{k}}$ . These expressions reduce to the AG-level results in the lowest order (Born limit).

It should be pointed out [4] that here  $\Delta$  is the excitation gap, related to the order parameter  $\Delta_{sc}$  and pseudogap  $\Delta_{pg}$  via  $\Delta^2 = \Delta_{sc}^2 + \Delta_{pg}^2$ .

Shown in Fig. 1 are the Feynman diagrams for the impurity  $T$ -matrices  $T_\omega$  and  $T_{\Delta^\dagger}$ , respectively, where  $T_{\Delta^\dagger}$  is the complex conjugate of  $T_\Delta$ . Note that for the impurity potential we use here, with  $u(\mathbf{k}, \mathbf{k}') = u$ , the impurity  $T$ -matrices

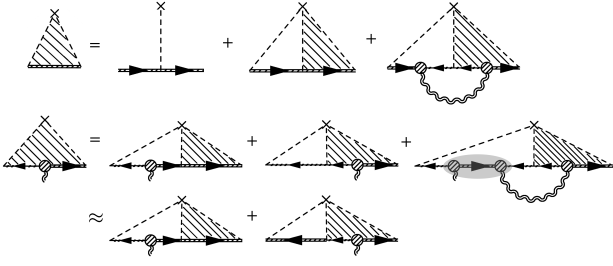


Figure 1: Feynman diagrams for the regular impurity  $T$ -matrix  $T_\omega$  and the anomalous impurity  $T$ -matrix  $T_{\Delta^\dagger}$ . The crosses denote the impurities and the dashed lines represent the impurity potential. The dressed thin solid, thick solid lines represent impurity dressed non-interacting and interacting fermion propagators, respectively. The shaded elliptical region denotes self-consistent impurity dressing of the double pairing vertex structure. See Ref. [4] for details.

only acquire a dynamical structure and are independent of the fermion momentum. Thus,  $T_\omega$  and  $T_\Delta$  can be decoupled as

$$T_\omega = \frac{u(1 - u\bar{G}_{-\omega})}{(1 - u\bar{G}_\omega)(1 - u\bar{G}_{-\omega}) + u^2\bar{F}_\omega\bar{F}_\omega^\dagger}, \quad (4a)$$

and

$$T_{\Delta^\dagger}(\omega - \Omega, \omega|Q) = \frac{u^2 \sum_{\mathbf{k}} G_0(Q - K) \Gamma_0(K|Q) G(K)}{(1 - u\bar{G}_\omega)(1 - u\bar{G}_{-\omega}) + u^2\bar{F}_\omega\bar{F}_\omega^\dagger} \times \frac{1 - u\bar{G}_{-\omega}}{1 - u\sum_{\mathbf{k}} G(Q - K)}, \quad (4b)$$

where we have used a four-momentum notation,  $K \equiv (\mathbf{k}, i\omega_l)$ ,  $Q \equiv (\mathbf{q}, i\Omega_n)$ , with  $\omega_l$  and  $\Omega_n$  being the odd and even Matsubara frequencies, respectively. Here we have also defined the impurity averaged Green's functions  $\bar{G}_\omega = \sum_{\mathbf{k}} G(K)$  and  $\bar{G}_{-\omega} = \sum_{\mathbf{k}} G(-K)$ , and the anomalous Green's function  $\bar{F}_\omega$  (and its complex conjugate  $\bar{F}_\omega^\dagger$ ) as

$$\bar{F}_\omega^\dagger = \sum_{\mathbf{k}} F^\dagger(K) = \sum_{\mathbf{k}} \Delta \Gamma_0(K) G_0(-K) G(K), \quad (4c)$$

where  $\Gamma_0(K) = \tilde{\Delta}_{\mathbf{k}}/\Delta$  is the renormalized pairing vertex function. For isotropic impurity scattering,  $T_\omega$  and  $T_{\Delta^\dagger}$  are independent of momentum.

In the static limit,  $Q \rightarrow 0$ , the expression for  $T_{\Delta^\dagger}$  becomes

$$T_{\Delta^\dagger}(\omega) = \frac{u^2 \bar{F}_\omega / \Delta}{(1 - u\bar{G}_\omega)(1 - u\bar{G}_{-\omega}) + u^2 \bar{F}_\omega \bar{F}_\omega^\dagger}. \quad (4d)$$

Unlike the cases of  $d$ -wave [4] and  $p$ -wave pairing [17], where  $\bar{F}_\omega \equiv 0$  so that this gap renormalization vanishes, here for our  $s$ -wave pairing,  $\varphi_{\mathbf{k}} = 1$ , the gap renormalization is given by

$$\tilde{\Delta} = \Delta + \Sigma_\Delta = \Delta \Gamma_0(\omega), \quad (5)$$

where

$$\Gamma_0(\omega) = 1 + n_i T_\Delta(\omega). \quad (6)$$

For the momentum independent vertex function in Eq. (6), using the expression for  $T_\Delta$  in Eq. (4d) and the impurity averaged Gor'kov function in Eq. (4c),  $\Gamma_0(\omega)$  can be written explicitly as

$$\Gamma_0(\omega) = \frac{1}{1 - n_i u^2 \lambda(\omega)}, \quad (7)$$

where

$$\lambda(\omega) = \frac{\sum_{\mathbf{k}} G(-K) G_0(K)}{\mathcal{D}_\omega}, \quad (8)$$

with

$$\mathcal{D}_\omega = (1 - u\bar{G}_\omega)(1 - u\bar{G}_{-\omega}) + u^2 \bar{F}_\omega \bar{F}_\omega^\dagger. \quad (9)$$

Finally, the full Green's function is given by

$$G(K) = \frac{i\tilde{\omega} - \epsilon_{\mathbf{k}}}{(i\tilde{\omega} - \epsilon_{\mathbf{k}})(i\tilde{\omega} - \epsilon_{\mathbf{k}}) + \tilde{\Delta}_{\mathbf{k}}^* \tilde{\Delta}_{\mathbf{k}}}. \quad (10)$$

## B. Analytical continuation and spectral representation

In order to numerically calculate the impurity renormalization functions, the Matsubara frequencies need to be analytically continued to the real frequencies,  $i\omega_l \rightarrow \omega + i0^+$ . In general, we have  $i\tilde{\omega} \neq -i\tilde{\omega}$ , due to the absence of the particle-hole symmetry. Therefore, both the positive and negative frequencies should be analytically continued at the same time. For  $l > 0$ ,  $i\tilde{\omega}_l \rightarrow \omega_+^R = \omega_+ + i\Sigma_+''$ , and  $i\tilde{\omega}_{-l} \rightarrow \omega_-^A = \omega_- - i\Sigma_-''$ . For  $l' < 0$ ,  $i\tilde{\omega}_{l'} \rightarrow \omega_-^R = \omega_- + i\Sigma_-''$  and  $i\tilde{\omega}_{-l'} \rightarrow \omega_+^A = \omega_+ - i\Sigma_+''$ . Here  $\omega_\pm = \pm\omega - \Sigma'_\pm$ , and we choose  $\omega > 0$  and  $\Sigma'_\pm > 0$ . The superscripts  $R$  and  $A$  denote retarded and advanced analytical continuations, respectively. We obtain

$$\begin{aligned} \bar{G}_{\omega>0}^R &= \sum_{\mathbf{k}} \frac{\omega_- - i\Sigma_-'' - \epsilon_{\mathbf{k}}}{(\omega_+ + i\Sigma_+'' - \epsilon_{\mathbf{k}})(\omega_- - i\Sigma_-'' - \epsilon_{\mathbf{k}}) + \Delta^2 |\Gamma_0^R(\omega)|^2}, \\ \bar{G}_{-\omega<0}^R &= \sum_{\mathbf{k}} \frac{\omega_+ - i\Sigma_+'' - \epsilon_{\mathbf{k}}}{(\omega_- + i\Sigma_-'' - \epsilon_{\mathbf{k}})(\omega_+ - i\Sigma_+'' - \epsilon_{\mathbf{k}}) + \Delta^2 |\Gamma_0^R(\omega)|^2}, \\ \Sigma_{\omega>0}^R &= \frac{n_i u (1 - u\bar{G}_{-\omega}^R)}{\mathcal{D}_\omega^R} = \Sigma'_+ - i\Sigma_+'', \\ \Sigma_{-\omega<0}^R &= \frac{n_i u (1 - u\bar{G}_\omega^R)}{\mathcal{D}_\omega^R} = \Sigma'_- - i\Sigma_-'', \end{aligned} \quad (11)$$

where  $\epsilon_{\mathbf{k}} = \mathbf{k}^2/(2m) - \mu$  with  $\mu$  being the chemical potential, and  $|\Gamma_0^R(\omega)|^2 = \Gamma_0^R(\omega)\Gamma_0^A(\omega) = \Gamma_0'^2(\omega) + \Gamma_0''^2(\omega)$ . From Eq. (7), we have

$$\Gamma_0^R(\omega) = \Gamma_0'(\omega) + i\Gamma_0''(\omega) = \frac{1}{1 - n_i u^2 \lambda^R(\omega)}, \quad (12)$$

where  $\lambda^R(\omega)$  can be calculated from Eqs. (8)-(10). Note that here the gap renormalization function  $\Gamma_0(\omega)$  involves pairing between four-momenta  $\pm K$ . Therefore, we have the symmetry  $\Gamma_0^*(\omega) = \Gamma_0(-\omega)$ . This is different from the frequency renormalization  $\Sigma_\omega$ .

Equations (11) and (12) form a closed set for solving for the six variables  $\Sigma'_{\pm\omega}, \Sigma''_{\pm\omega}, \Gamma'_0(\omega), \Gamma''_0(\omega)$  as a function of  $\omega$ . In comparison with the  $d$ -wave case in Ref. [4], here we have two more extra equations to solve.

For the 3D Fermi gas and the contact impurity potential we consider here, the real part of  $\bar{G}_\omega^R$  diverges, caused by the momentum integral over  $\mathbf{k}$  far away from the Fermi surface. In the AG theory, this ultraviolet divergence is absorbed into the chemical potential  $\mu$ , signifying an additive correction,  $\delta\mu$ , to the chemical potential [12]. Here we adopt a similar regularization scheme, and replace  $\bar{G}_\omega^R$  with

$$\bar{\mathcal{G}}_\omega^R = \bar{G}_\omega^R - \bar{G}_{\omega=0}^R. \quad (13)$$

It is easy to show that  $\bar{\mathcal{G}}_{\omega=0}^R$  is real and thus can be fully absorbed into a renormalized chemical potential. In the lowest order (Born limit),  $\mathcal{D}_\omega \approx 1$  and  $\Sigma_\omega \sim n_i u^2 \bar{\mathcal{G}}_{\omega=0}^R$ , so that our regularization scheme reduces to that of the AG theory, with  $\delta\mu \sim n_i u^2 \bar{\mathcal{G}}_{\omega=0}^R$ . Beyond the Born limit, the corrections to  $\Sigma_\omega$  and  $\Gamma_0(\omega)$  caused by the regularization are proportional to  $1/\bar{\mathcal{G}}_{\omega=0}^R$  and  $1/(\bar{\mathcal{G}}_{\omega=0}^R)^2$ , respectively, which are negligible.

With the renormalization functions  $\Sigma_\omega$  and  $\Gamma_0(\omega)$ , one can calculate the pair susceptibility

$$\chi(Q) = \sum_K \Gamma_0(K|Q) G(K) G_0(Q - K), \quad (14)$$

whose real and imaginary parts are given respectively by

$$\begin{aligned} \chi'(\Omega + i0^+, \mathbf{q}) &= \text{Im} \sum_{\mathbf{k}} \int_{-\infty}^{\infty} \frac{d\omega}{2\pi} \left\{ G^R(\omega, \mathbf{k}) G_0^R(\Omega - \omega, \mathbf{q} - \mathbf{k}) \right. \\ &\quad \times [f(\omega - \Omega) - f(\omega)] + G^R(\omega, \mathbf{k}) G_0^A(\Omega - \omega, \mathbf{q} - \mathbf{k}) \\ &\quad \times [1 - f(\omega) - f(\omega - \Omega)] \left. \right\} \Gamma_0^R(\omega|Q), \end{aligned} \quad (15a)$$

and

$$\begin{aligned} \chi''(\Omega + i0^+, \mathbf{q}) &= -\text{Im} \sum_{\mathbf{k}} \int_{-\infty}^{\infty} \frac{d\omega}{2\pi} G^R(\omega, \mathbf{k}) A_0(\Omega - \omega, \mathbf{q} - \mathbf{k}) \\ &\quad \times [f(\omega - \Omega) - f(\omega)] \Gamma_0^R(\omega|Q), \end{aligned} \quad (15b)$$

where  $f(\omega)$  is the Fermi distribution function. Here  $\Gamma_0^R(\omega|Q)$  can be obtained from Eq. (4b) after analytical continuation, with  $\Gamma_0^R(\omega|0) = \Gamma_0^R(\omega)$ . And  $A_0(\omega, \mathbf{k}) = -2 \text{Im} G_0^R(\omega, \mathbf{k})$  is the “bare” spectral function.

For  $Q = 0$ , we obtain

$$\chi(0) = \text{Im} \sum_{\mathbf{k}} \int_0^\infty \frac{d\omega}{\pi} \frac{[1 - 2f(\omega)] \Gamma_0^R(\omega)}{C(\omega, \mathbf{k})}, \quad (16)$$

where  $C(\omega, \mathbf{k}) = (\omega_+ + i\Sigma_+'' - \epsilon_{\mathbf{k}})(\omega_- - i\Sigma_-'' - \epsilon_{\mathbf{k}}) + \Delta^2 |\Gamma_0^R(\omega)|^2$ .

Substituting into the Thouless criterion,  $1 + g\chi(0) = 0$ , we have the gap equation

$$-\frac{m}{4\pi a} = \sum_{\mathbf{k}} \left[ \text{Im} \int_{-\infty}^{\infty} \frac{d\omega}{2\pi} \frac{[1 - 2f(\omega)] \Gamma_0^R(\omega)}{C(\omega, \mathbf{k})} - \frac{1}{2\epsilon_{\mathbf{k}}^0} \right], \quad (17)$$

where we have used the Lippmann-Schwinger equation (1) to replace  $g$  with scattering length  $a$ .

Now the fermion number equation becomes

$$\begin{aligned} n &= 2 \sum_{\mathbf{k}} \int_{-\infty}^{\infty} \frac{d\omega}{2\pi} A(\mathbf{k}, \omega) f(\omega) \\ &= \int_{-\infty}^{\infty} \frac{d\omega}{\pi} N(\omega) f(\omega), \end{aligned} \quad (18)$$

where  $A(\mathbf{k}, \omega) = -2 \text{Im} G^R(\omega, \mathbf{k})$  is the renormalized spectral function and

$$N(\omega) = \sum_{\mathbf{k}} A(\mathbf{k}, \omega) = -2 \text{Im} \bar{\mathcal{G}}_\omega^R \quad (19)$$

is the density of states. Next we evaluate the pseudogap, which is given by

$$\Delta_{pg}^2 = - \sum_{\mathbf{q}} \int_{-\infty}^{\infty} \frac{d\Omega}{\pi} \text{Im} t^R(Q) b(\Omega), \quad (20)$$

where  $b(x)$  is the Bose distribution function, and the retarded  $T$  matrix  $t^R(Q) = [\chi(\Omega + i0^+, \mathbf{q}) - \chi(0, \mathbf{0})]^{-1}$ . In actual numerics, we follow Ref. [4] and Taylor expand the inverse  $T$  matrix,  $t^{-1}(\Omega + i0^+, \mathbf{q})$ , which greatly facilitates the computation.

### III. NUMERICAL RESULTS

The numerics is done as follows. First, for given (initial) values of the parameters  $[\mu, T_c, \Delta]$ , the renormalization spectrum  $\Sigma_\omega$  and  $\Gamma_0(\omega)$  are solved. Next, these renormalization functions are substituted into the gap, pseudogap and fermion number equations and an equation solver is used to obtain  $\mu(T_c)$ ,  $T_c$ , and  $\Delta(T_c)$  at  $T_c$  and gap, order parameter as well as  $\mu$  below  $T_c$ . With these newly obtained parameters, the equation solver will repeat the above process, until self-consistent solutions are obtained.

#### A. Impurity renormalization functions and the density of states

In this subsection, we numerically solve the the coupled equations for  $[\Sigma'_\pm, \Sigma''_\pm, \Gamma'_0, \Gamma''_0]$  as a function of  $\omega$  for given impurity levels and study the impurity renormalization effects on the frequency and gap function, as well as the DOS.

We first present in Fig. 2 typical (a) frequency and (b) gap (pairing vertex) renormalization functions  $\Sigma_\omega$  and  $\Gamma_0(\omega)$ , respectively. Shown here are the functions for a unitary Fermi gas at an intermediate impurity level  $n_i/n = 5\%$  and impurity scattering strength  $u/E_F = 20$ , which is close to the unitary scattering limit. The real (Re) and imaginary (Im) parts of  $\Sigma_\omega$  and  $\Gamma_0(\omega)$  are solved at the same time, as explained above. The frequency axis is plotted in units of the clean gap  $\Delta = 0.64 E_F$ . From Fig. 2(a), one can easily spot an impurity band (IB) near  $\omega \simeq -3\Delta$ , which manifests as a broad peak

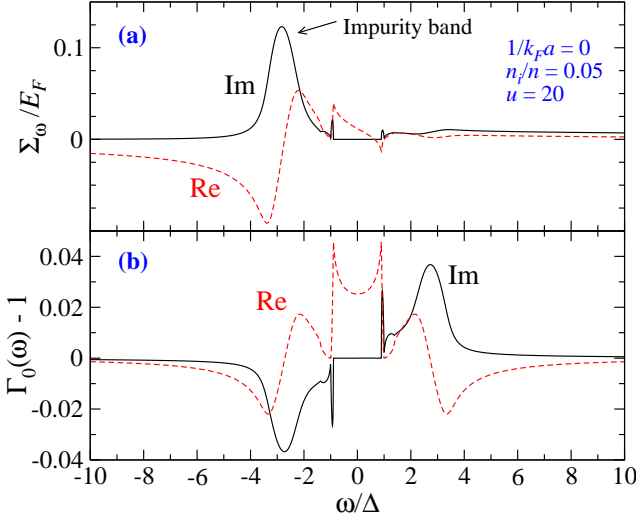


Figure 2: The impurity renormalization functions  $\Sigma_\omega$  and  $\Gamma_0(\omega)$ , in a unitary Fermi gas at an intermediate impurity scattering level, with  $n_i = 0.05n$ ,  $u/E_F = 20$ . Re (Im) denotes the real (imaginary) part of the functions. There are sharp features near  $\omega = \pm\Delta$ . The broad peak of  $\Sigma''_\omega$  at  $\omega/\Delta \approx -3$  (black curve) indicates the formation of an impurity band. The horizontal axes are rescaled by the gap  $\Delta$  of a clean system.

in  $\Sigma''(\omega)$ . The peak location is given by the zero point of  $\text{Re } \mathcal{D}_\omega$ , leading to a peak in  $\Gamma_0''(\omega)$  as well, which shares the same denominator. Interestingly, even for positive  $u$ , the IB may occur on the negative  $\omega$  side as well, due to the presence of a nonzero  $\bar{F}_\omega$  in  $\mathcal{D}_\omega$  and particle-hole mixing. Indeed, as one can easily see from Eq. (4a), for large  $|u|$ , the sign of  $u$  becomes almost irrelevant. This should be contrasted to the  $d$ -wave case in Ref. [4]. There are sharp features related to the pairing gap edge at  $\omega = \pm\Delta$ , esp. in the pairing vertex renormalization function  $\Gamma_0(\omega)$ . With the impurity configuration in Fig. 2, inside the gap (i.e.,  $|\omega| < \Delta$ ), the imaginary parts of both  $\Sigma_\omega$  and  $\Gamma_0(\omega)$  are essentially zero. In addition, as expected, the impurity renormalization effects are mostly in the low frequency regions, and decreases with a power law of  $|\omega|$  at sufficient high frequencies. Note that for clarity, here we plot  $\Gamma_0(\omega) - 1$  in Fig. 2(b), as the renormalization is small in comparison to its unrenormalized value,  $\Gamma_0(\omega) = 1$ . As a consistency check, we note that Fig. 2(b) obeys the symmetry  $\Gamma_0(-\omega) = \Gamma_0^*(\omega)$ .

As can be seen from Fig. 2, the real part of the impurity scattering is in general small compared to the unrenormalized part. For the frequency,  $\Sigma'_\pm$  constitutes only a small perturbation to  $\omega$ , so that the main impurity effect resides in the imaginary parts. Inside the main band ( $\omega > -\sqrt{\mu^2 + \Delta^2}$ ), a large  $\Sigma'_\pm$  means a large spectral weight loss, whereas outside the main band, it means a large spectral weight gain. The imaginary parts increase with the impurity density  $n_i$ .

For weak scattering in the Born limit, the impurity band does not exist. Only when the scattering strength  $|u|$  becomes large enough are there significant spectral weight gain outside the main band. The location of the impurity band (if it exists)

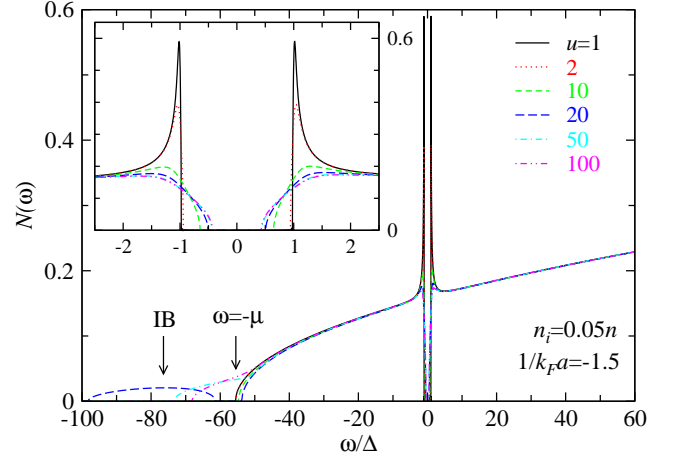


Figure 3: Effects of different impurity scattering strength  $u$  from the Born limit  $u/E_F = 1$  to the unitary limit  $u/E_F = 100$  on the fermion DOS  $N(\omega)$  in the BCS regime ( $1/k_F a = -1.5$ ), with impurity density  $n_i = 0.05n$ . The impurity band (IB) splits from the main band (blue curve) for an intermediate value of  $u/E_F = 20$ . The inset presents the details of the coherence peaks, sharing the same axis labels. Here  $\Delta \approx 0.018E_F$ .

is largely determined by the impurity strength  $u$ , whereas the impurity density  $n_i$  affects the magnitude of  $\Sigma''(\omega)$  and  $\Gamma_0''(\omega)$  and the spectral weight of the impurity band. The impurity band becomes prominent only when it is located outside the main band. In the BCS regime, the gap  $\Delta$  becomes small. Once the impurity band is clearly visible, it will appear on the far left side in a plot such as Fig. 2.

Next we show in Fig. 3 the effects of an increasing impurity scattering strength  $u$  on the DOS  $N(\omega)$  for  $1/k_F a = -1.5$  in the BCS regime, where the gaps are relatively small, from the Born limit  $u/E_F = 1$  to the unitary scattering limit  $u/E_F = 100$ . Here we choose a representative, intermediate impurity density,  $n_i = 0.05n$ . We show details of the coherence peak in the inset. The location  $\omega = -\mu$  indicates roughly the bottom of the main band. It is evident that weak scatterers are not effective in destroying the coherence peaks. Indeed, this is in agreement with the Anderson's theorem for weak impurities based on the AG level treatment. However, when the impurity strength  $u$  increases, say, beyond 10, the coherence peaks become smeared out quickly, and significant spectral weight is now moved inside the gap. For sufficiently strong  $u$  and high density  $n_i$ , the gap will be filled up so that the superfluidity is destroyed. This should also be compared with the  $d$ -wave case, where impurities in the Born limit are found to be effective in smearing out the coherence peaks [4]. Note that as mentioned earlier, the sign of  $u$  is nearly irrelevant for our short-range  $s$ -wave pairing. Therefore, we plot here only curves for positive  $u$ .

One prominent feature in Fig. 3 is the presence of the impurity band for large  $u$ . More interestingly, the location of the band does not move monotonically to the negative frequencies with increasing  $u$ . In Fig. 3, the IB is well split from the main band for  $u = 20$  (blue dashed curve), but partially overlaps

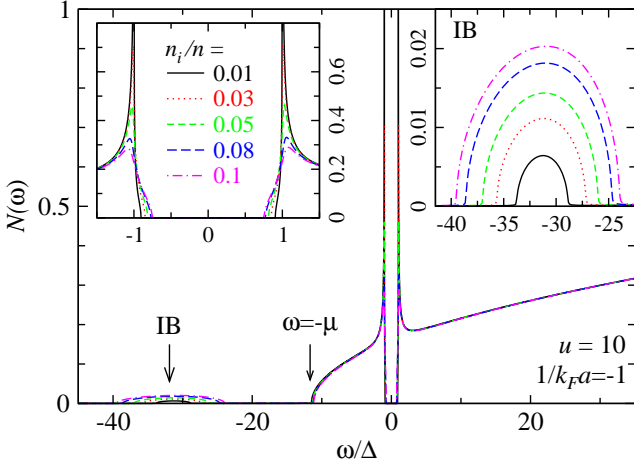


Figure 4: Effects of impurity scattering on the fermion DOS in the BCS regime ( $1/k_F a = -1$ ), with impurity scattering strength  $u = 10E_F$  and impurity density varying from  $n_i = 0.01n$  to  $n_i = 0.1n$ . Detailed structure of  $N(\omega)$  near the gap edge, and the impurity band are shown in the left and right insets, respectively. Here  $\Delta \approx 0.085E_F$ .

with the main band for the larger  $u = 50$  (cyan dot-dashed) and  $u = 100$  (magenta double-dot-dashed curve). Such a non-monotonic behavior was not seen for the  $d$ -wave case [4].

Shown in Fig. 4 are the effects of increasing impurity density  $n_i/n$  from 0.01 to 0.1 on the DOS  $N(\omega)$  for  $1/k_F a = -1$  in the BCS regime, with a fixed  $u = 10E_F$ . Shown in the left and right insets are the magnified view of  $N(\omega)$  for the coherence peaks and the impurity band below the main band. Here the IB is well separated from the main band, with spectral weight given by  $2n_i$ . The increasing impurity density also serves to smear out and suppress the coherence peaks. For sufficient high impurity  $n_i$ , the superfluidity will be destroyed. When comparing the coherence peaks for the  $n_i/n = 0.05$  and  $u/E_F = 10$  case between Figs. 3 and 4, it is easy to conclude that a larger gap is more robust against impurity scattering.

In Fig. 5 we show the effects of varying impurity scattering strength  $u$  on the DOS in the (a) unitary and (b) BEC regimes, respectively, with impurity density  $n_i/n = 0.05$ . With substantially larger gaps, the DOS in these two regimes are very robust against impurity effects. Indeed, only minor smearing of coherence peak can be found in the unitary case in Fig. 5(a). For the BEC case with  $1/k_F a = 1$  in Fig. 5(b), the chemical potential  $\mu/E_F = -0.80$  is negative, so that there exists no underlying Fermi surface. As a result, there are no coherence peaks in the clean limit. The spectral weight below the bottom of the main band is mainly a result of particle-hole mixing in both cases, with a power law tail  $N(\omega) \propto |\omega|^{-3/2}$  towards  $\omega \rightarrow -\infty$ . Nevertheless, signatures of impurity band on top of this power law tail can be seen for  $u/E_F = 10$  (green dotted) and 20 (blue dashed curves). In addition, it is clear that a larger  $u$  is more effective in moving the spectral weight to within the gaps. Though the DOS in these two regimes is not as sensitive to impurities as in BCS regime, the finite  $\Sigma(\omega)$

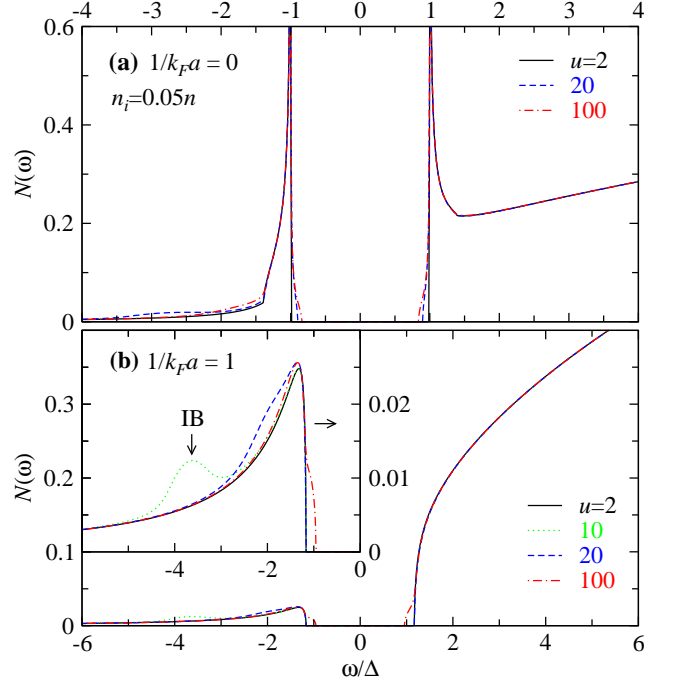


Figure 5: Effects of impurity scattering on the fermion DOS at (a)  $1/k_F a = 0$  and (b) 1, corresponding to unitary and BEC cases, respectively, with the impurity density  $n_i = 0.05n$ , for different impurity scattering strength  $u$  varying from the Born limit  $u/E_F = 2$  to the unitary limit  $u/E_F = 100$ . Here  $(\mu/E_F, \Delta/E_F) = (0.62, 0.64)$  and  $(-0.80, 1.33)$ , and the main band bottom is located at  $\omega/\Delta \approx -1.4$  and  $1.17$  for (a) and (b), respectively.

and  $\Gamma_0(\omega)$  as well as the finite fermion pair lifetime (caused by impurities) may also affect the superfluid  $T_c$  and other superfluid properties.

## B. Effects of impurities on the behavior of $T_c$ in $s$ -wave BCS-BEC crossover

In this subsection we present the effects of impurities on  $T_c$  throughout BCS-BEC crossover. Plotted in Fig. 6 is the behavior of  $T_c$  as a function of  $1/k_F a$  from the BCS through BEC regimes. For clarity, here we show only one case with a representative impurity density  $n_i = 0.05n$  in the unitary scattering regime,  $u/E_F = 100$  (red solid curve). For comparison, we also show the  $T_c$  curve in the clean system (black dotted line) as well as the mean field result (blue dashed line). As one can expect from previous figures,  $T_c$  is suppressed by impurity scattering. Furthermore, the relative suppression is much stronger in the BCS regime than in the unitary and BEC regimes. In the deep BCS regime,  $T_c$  is suppressed down to zero by strong impurities, leading to an effective power law dependence of  $T_c$  on  $1/k_F a$  in the BCS regime [19]. In the pseudogap or crossover regime, the maximum  $T_c$  now shifts to the BEC side of the Feshbach resonance (where  $1/k_F a = 0$ ). This result is somewhat similar to the shift of the  $T_c$  curve by particle-hole fluctuations [20], suggesting that even “nonmag-

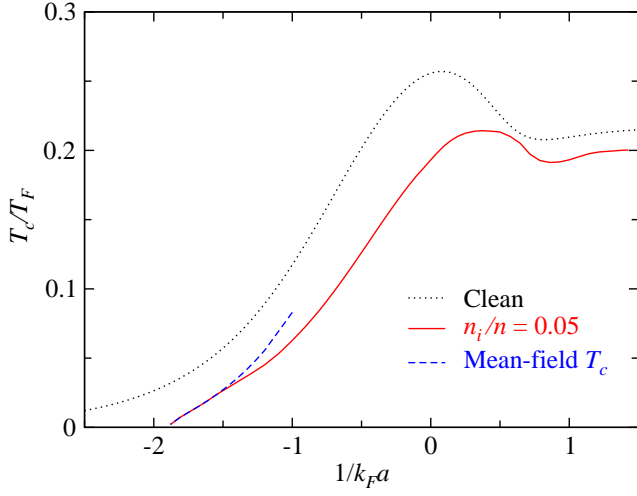


Figure 6: Behavior of  $T_c$  throughout the BCS-BEC crossover in the clean limit (black dotted line) and in the presence of strong impurity scattering with density  $n_i = 0.05n$  and strength  $u = 100E_F$  (red solid line). For comparison, also plotted is the mean field value of  $T_c$  with the impurities (blue dashed line).

netic” impurities may to certain extent have a pair-breaking effect. On the other hand, impurity scattering and particle-hole fluctuations are very different. In the BCS regime, while the latter simply reduces  $T_c$  by a factor of 0.45, here strong impurities in the unitary regime can destroy superfluidity completely whereas weak impurities in the Born limit (not shown) may leave  $T_c$  intact. The result shown in Fig. 6 should be contrasted with the  $d$ -wave case [4]. Due to the sign change of the order parameter across the nodes in the momentum space, impurity scattering is much more effective in destroying  $T_c$  throughout the entire BCS-BEC crossover. For example, Anderson’s theorem for weak impurities only works for  $s$ -wave superfluids as we study here.

Next, we study the effects of impurity scattering strength on  $T_c$ . Shown in Fig. 7 is  $T_c$  as a function of  $u/E_F$ , from  $-\infty$  to  $+\infty$ , for a unitary Fermi gas, with a representative impurity density  $n_i = 0.05n$ . Here the impurity strength  $u$  spans from the Born limit to the unitary limit, for both attractive and repulsive scatterers. The  $T_c$  value in the  $u \rightarrow 0$  limit is slightly higher than the clean system value,  $T_c^0/T_F \approx 0.256$  [20], due to the subtraction of  $\bar{G}_{\omega=0}^R$  from  $\bar{G}_\omega^R$  in Eq. (13). In the Born regime,  $T_c$  decreases slowly with increasing  $|u|$ . Once  $|u|$  increases further away from the Born limit,  $T_c$  decreases rapidly (as  $\gamma \propto u^2$ ) at first, then slows down and eventually approaches a constant in the unitary scattering limit. Such asymptotic behavior is indeed consistent with the expressions for  $\Sigma_\omega$  and  $\Gamma_0(\omega)$  in Eqs. (11)-(12), from which one can readily show that in the large  $|u|$  limit both  $\Sigma_\omega$  and  $\Gamma_0(\omega)$  becomes essentially  $u$  independent. The suppression of superfluidity and  $T_c$  by strong impurity scattering is basically caused by two effects. On the one hand, strong impurity scattering leads to a finite lifetime of fermionic quasiparticles, and thus depletes DOS in the coherence peak and transfers spectral weight to the impurity band and subgap states; such a

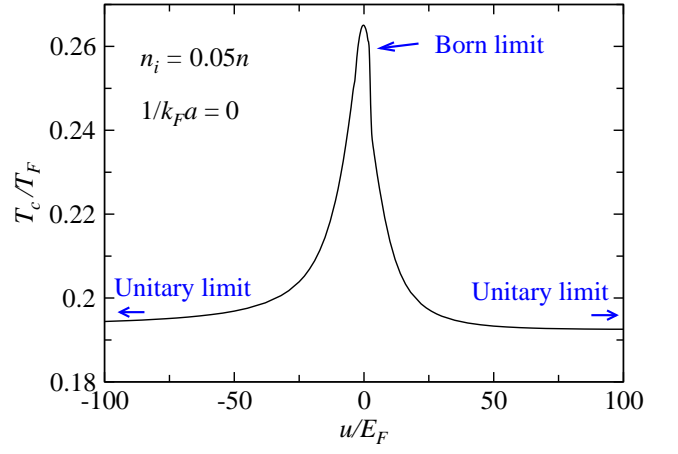


Figure 7: Superfluid transition temperature  $T_c$  of a unitary Fermi gas as a function of impurity scattering strength  $u$ , from the Born limit through the unitary limit, with an impurity density  $n_i = 0.05n$ .

spectral weight relocation is detrimental to superfluidity. On the other hand, the impurity scattering also causes a finite lifetime of fermion pairs. While the former is dominant in the BCS regime, the latter dominates the BEC side.

Note that the  $T_c$  curve in Fig. 7 is almost symmetric about  $u = 0$ , consistent with Eqs. (4). This should be contrasted to the case of  $d$ -wave superfluidity, where such a symmetry is clearly absent due to vanishing  $\bar{F}_\omega$  [4].

### C. Gaps and the superfluid density in the presence of impurities

Now we investigate the transport properties of a Fermi gas in the presence of impurities. The superfluid density can be derived using a linear response theory. Following Ref. [4], for  $s$ -wave pairing with  $\varphi_{\mathbf{k}} = 1$  in three dimensions, we obtain

$$\frac{n_s}{m} = \frac{4}{3} \Delta_{sc}^2 \sum_{\mathbf{k}} \int_{-\infty}^{\infty} \frac{d\omega}{\pi} \text{Im} \left( \tilde{F}^A(\omega, \mathbf{k}) \right)^2 (\vec{\nabla}_{\epsilon_{\mathbf{k}}})^2 |\Gamma_0^R(\omega)|^2 f(\omega), \quad (21)$$

where  $\tilde{F}^A(\omega, \mathbf{k}) = 1/C^*(\omega, \mathbf{k})$ , different from  $F(K)$  by a factor  $\tilde{\Delta}_{\mathbf{k}}$ , and  $C(\omega, \mathbf{k})$  is given in Sec. II B.

First we plot in Fig. 8(a) the gaps and the order parameter  $\Delta_{sc}$  as a function of  $T/T_c^0$  in a unitary Fermi gas, where  $T_c^0$  is the clean system superfluid transition temperature. We choose strong impurities in the unitary limit, with  $u = 100E_F$ , and calculate for three representative impurity densities of  $n_i/n = 0$  (clean, black solid curve), 0.03 (red dotted curve), 0.05 (blue dashed curve), respectively. For clarity, we show the pseudogap  $\Delta_{pg}$  and the total excitation gap  $\Delta$  only for the  $n_i/n = 0.05$  case. It is easy to conclude that unitary impurities significantly suppresses both  $T_c$  and the gaps, including the order parameter. In addition, the suppression is more effective for  $T_c$  than for the gaps. This can also be seen from



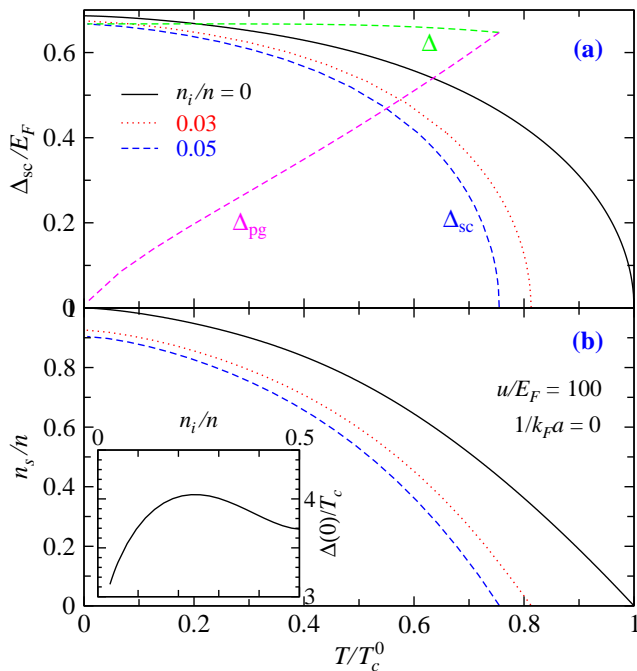


Figure 8: (a) Superfluid gaps and order parameter  $\Delta_{sc}$  and (b) superfluid density  $n_s/n$  in a unitary Fermi gas, as a function of  $T/T_c^0$ , for different densities of impurity, including the clean limit (black solid line) and  $n_i/n = 0.03$  (red dotted) and  $0.05$  (dashed lines), with scattering strength  $u/E_F = 100$ . For clarity, we show the total gap  $\Delta/E_F$  and the pseudogap  $\Delta_{pg}/E_F$  only the  $n_i/n = 0.05$  case. Shown in the inset is a continuous evolution of the corresponding ratio  $\Delta(0)/T_c$  vs  $n_i/n$ . Here  $T_c^0/T_F = 0.256$  is the  $T_c$  in the clean limit.

the ratio  $\Delta(0)/T_c$  as a function of  $n_i/n$ , as shown in the inset; the ratio initially increases rapidly with  $n_i$ , and drops slightly after reaching a maximum. Such a non-monotonic and non-constant behavior signals the breakdown of Anderson’s theorem for strong impurities. We note here that this ratio is rather different from the mean-field value of 1.76, due to primarily the presence of a pseudogap at  $T_c$  besides the impurity effects.

With the calculated gap parameters, we show the corresponding calculated superfluid density as a function of temperature for the above the three impurity densities in Fig. 8(b). As with the order parameter, the superfluid density is suppressed effectively by impurities in the unitary limit. While the reduction of  $n_s$  increases with  $n_i$ , nonlinearity is clearly present. Detailed study of  $n_s$  versus  $n_i$  at zero  $T$  is shown in Fig. 9. Similar to the  $d$ -wave case on a lattice [4], here we also find that for unitary scatterers ( $u = 100E_F$ ),  $n_s$  drops initially very fast with  $n_i$  and then slows down as  $n_i$  increases further. In contrast, for Born scatterers ( $u = 3E_F$ ),  $n_s$  decreases roughly linearly with  $n_i$ . It should be noted that due to the large gap size at unitarity, it takes a large  $n_i/n$  in both cases to destroy the superfluid completely. While the theory may break down at such a large impurity density, it does indicate the robustness of an  $s$ -wave unitary Fermi gas against impurity scattering, as compared to a weak coupling BCS case (see e.g., Fig. 6) or the  $d$ -wave case shown in Ref. [4].

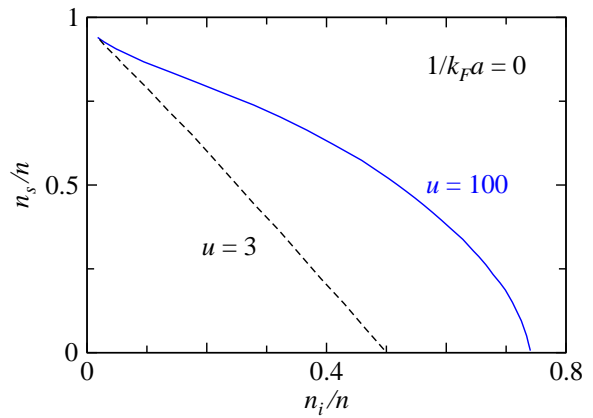


Figure 9: (a) Fractional superfluid density  $n_s/n$  in a unitary Fermi gas at  $T = 0$  as a function of the relative impurity density  $n_i/n$ , for both unitary (blue solid) and Born (black dashed curves) scatterers.

Finally, we note that it requires some effort to realize a homogeneous Fermi gas in the presence of impurities. First, atomic Fermi gases are always confined in a trapping potential. The impurities should be confined within this trapping potential as well. To improve the situation, one may use a combination of different lasers to create a rather flat trap to make the system as close to homogeneous as possible. Second, while the impurities may be realized by doping with heavy atoms, a more elaborate treatment may need to consider the finite mass of these impurity atoms. In this way, a different impurity scattering Hamiltonian will have to be used. Third, an alternative to realize impurities is to create (pseudo-)randomly distributed optical speckles in the trap. In this case, these speckles may be regarded as infinitely heavy impurities so that the scattering of atoms is elastic, as assumed in our theory. Nevertheless, the present theory can be regarded as a first step toward a more realistic treatment of a real Fermi gas system with random impurities. Spin flip (i.e., “magnetic”) impurity scattering will also be considered in future works. Furthermore, we shall also include the particle-hole channel contributions [20] as well.

#### IV. SUMMARY

In summary, we have studied the effects of impurities on the  $s$ -wave BCS-BEC crossover in ultracold atomic Fermi gases, including the impurity effects on frequency and gap renormalizations, fermion density of states, superfluid  $T_c$ , as well as finite temperature gaps and superfluid density. Our results reveal that while the system is less sensitive to impurities in the Born limit, strong impurities in the unitary scattering regime cause a much stronger renormalization for both the frequency and the gaps throughout the entire BCS-BEC crossover, leading to a finite lifetime of Bogoliubov quasiparticles and fermion pairs, and hence a significant suppression of the superfluid  $T_c$  and superfluid density. The Anderson’s theorem breaks down except for weak impurities in the BCS regime. Indeed, in the weak coupling BCS regime, where the



gap is small, strong impurities at moderately high densities may readily destroy the superfluidity and suppress  $T_c$  down to zero, leading to an effective power law dependence on the pairing strength. Such a BCS-BEC crossover phenomenon in the presence of impurities may be realized experimentally by introducing atoms of foreign elements or using optical speckles, with Feshbach resonance in Fermi gases of  $^6\text{Li}$  or  $^{40}\text{K}$ .

### Acknowledgments

This work is supported by NSF of China (Grant No. 11274267), the National Basic Research Program of China

(Grants No. 2011CB921303 and No. 2012CB927404), and NSF of Zhejiang Province of China (Grant No. LZ13A040001).

- 
- [1] Q. J. Chen, J. Stajic, S. N. Tan, and K. Levin, Phys. Rep. **412**, 1 (2005).
  - [2] A. A. Abrikosov and L. P. Gor'kov, Sov. Phys. JETP **8**, 1090 (1959).
  - [3] S. H. Pan, E. W. Hudson, K. M. Lang, H. Eisaki, S. Uchida, and J. C. Davis, Nature **403**, 746 (2000).
  - [4] Q. J. Chen and J. R. Schrieffer, Phys. Rev. B **66**, 014512 (2002).
  - [5] B. Sacepe, T. Dubouchet, C. Chapelier, M. Sanquer, M. Ovdadia, D. Shahar, M. Feigel'man, and L. Ioffe, Nat. Phys. **7**, 239 (2011).
  - [6] K. Bouadim, Y. L. Loh, M. Randeria, and N. Trivedi, Nat. Phys. **7**, 884 (2011).
  - [7] Y. Dubi, Y. Meir, and Y. Avishai, Nature **449**, 876 (2007).
  - [8] M. V. Feigel'man and M. A. Skvortsov, Phys. Rev. Lett. **109**, 147002 (2012).
  - [9] H. Ding, T. Yokoya, J. Campuzano, T. Takahashi, M. Randeria, M. R. Norman, T. Mochiku, K. Kadowaki, and J. Giapintzakis, Nature **382**, 51 (1996).
  - [10] L. Han and C. A. R. Sa de Melo, New J. Phys. **13**, 055012 (2011).
  - [11] L. Sanchez-Palencia and M. Lewenstein, Nat. Phys. **6**, 87 (2010).
  - [12] A. A. Abrikosov, L. P. Gor'kov, and I. E. Dzyaloshinski, *Methods of Quantum Field Theory in Statistical Physics* (Dover Publications, New York, 1975).
  - [13] P. W. Anderson, J. Phys. Chem. Solids **11**, 26 (1959).
  - [14] G. Orso, Phys. Rev. Lett. **99**, 250402 (2007).
  - [15] P. Nozières and S. Schmitt-Rink, J. Low Temp. Phys. **59**, 195 (1985).
  - [16] F. Palestini and G. C. Strinati, Phys. Rev. B **88**, 174504 (2013).
  - [17] P. J. Hirschfeld, P. Wolfle, and D. Einzel, Phys. Rev. B **37**, 83 (1988).
  - [18] A. V. Balatsky, I. Vekhter, and J.-X. Zhu, Rev. Mod. Phys. **78**, 373 (2006).
  - [19] M. V. Feigel'man, L. B. Ioffe, V. E. Kravtsov, and E. A. Yuzbashyan, Phys. Rev. Lett. **98**, 027001 (2007).
  - [20] Q. J. Chen, Sci. Rep. **6**, 25772 (2016).